Tandem ion mobility spectrometry coupled to laser excitation

Anne-Laure Simon, Fabien Chirot, Chang Min Choi, Christian Clavier, Marc Barbaire, Jacques Maurelli, Xavier Dagany, Luke Macaleese, Philippe Dugourd

Tandem ion mobility spectrometry coupled to laser excitation

Anne-Laure Simon,[1] Fabien Chirot,[2] Chang Min Choi,[1] Christian Clavier,[1] Marc Barbaire,[1] Jacques Maurelli,[1] Xavier Dagany,[1] Luke MacAleese,[1] and Philippe Dugourd[1*]

[1] *Institut Lumière Matière, Université Lyon 1-CNRS, Université de Lyon 69622 Villeurbanne cedex, France*

[2] *Institut des Sciences Analytiques, Université Lyon 1-CNRS, Université de Lyon 69622 Villeurbanne cedex, France*

This manuscript describes a new experimental set-up that allows to perform tandem ion mobility spectrometry (IMS) measurements, and which is coupled to a high resolution time-of-flight mass spectrometer. It consists of two 79 cm long drift tubes (DT) connected by a dual ion funnel assembly. The set up was built to permit laser irradiation of the ions in the transfer region between the two drift tubes. This geometry allows selecting ions according to their ion mobility in the first drift tube, to irradiate selected ions and examine the ion mobility of the product ions in the second drift tube. Activation by collision is possible in the same region (between the two tubes) and between the second tube and the time-of-flight. IMS-IMS experiments on Ubiquitin are reported. We selected a given isomer of charge state +7 and explored its structural rearrangement following collisional activation between the two drift tubes. An example of IMS-Laser-IMS experiment is reported on eosin Y, where laser irradiation was used to produce radical ions by electron photodetachment starting from doubly deprotonated species. This allowed measuring the collision cross section of the radical photo-product, which cannot be directly produced with an electrospray source.

* philippe.dugourd@univ-lyon1.fr

I. INTRODUCTION

Ion mobility spectrometry (IMS) coupled to mass spectrometry (MS) plays an increasing role in analytical sciences, physical chemistry, as well as in structural biology. Since the electric mobility of an ion in a buffer gas depends on its geometry, IMS measurements allow resolving isomers or conformers that cannot be resolved by mass spectrometry [1-3]. In combination with molecular modeling it can help to elucidate the structure of ions and ion complexes [4-6]. IMS can also be used to observe structural rearrangements and to understand the different parameters that influence the folding and conformational stability of molecular ions such as peptides and proteins. Early works from Bowers, Jarrold and Clemmer [3, 7] reported conformational changes in response to temperature increase of the drift tube or collisional activation at the entrance of the tube. Dynamics studies in a drift tube are particularly attractive as the ions are embedded in a carrier gas (generally Helium or Nitrogen), which allows studies in the canonical (or grand canonical by addition of reactants) ensemble. For example, entropy and enthalpy for structural isomerization of salt clusters occurring inside the tube were determined by Dugourd et al [8]. The influence of desolvation and partial hydration on structural rearrangements of peptides and proteins was also reported [9-13] shedding a new light on hydrophobic forces.

Structural changes were further explored by Clemmer and coworkers with the development of instruments that incorporate multifield drift tube designs [14, 15] and by Hill and coworkers with combination of travelling wave and constant electric field drift tubes[16]. They allow selecting components from a mixture of ions on the basis of mobility differences prior to collisional activation inside the drift tube. The resulting ions that are produced can then be dispersed again in a second ion mobility spectrometry step (IMS^2 experiments). The second drift region is used either to separate fragment ions [15] or in the case of mild or no excitation to follow conformational changes starting from a well resolved isomer, providing information on conformational landscapes [17].

While both IMS and photofragmentation are two well established approaches for structural study of ions, few attempts have been made at coupling both techniques. Clemmer and Reilly [18-20] combined IMS separation with vacuum ultraviolet photodissociation and tandem MS. Incorporation of the mobility separation helps to distinguish isomers having identical *m/z* values prior to photofragmentation analysis. Laser excitation of isomer-resolved of carbon clusters [21] and of flavin mononucleotide [22] were also recently reported.

Several groups have worked on the coupling of spectroscopy with IMS. Photoelectron spectra of conformer selective cluster and biomolecule anions were reported [23-26]. UV and IR spectroscopy on selected ions was reported by von Helden [27] and Rizzo [28, 29] allowing elucidation of the structure of ubiquitin and bradykinin ions, respectively. The use of IMS to monitor photo-isomerization of molecular ions has been pioneered by Bieske and coworkers [30-32]. First report on cis-trans isomerization of diethylthiacarbocyanine was obtained using a single drift tube and on-axis laser excitation with a tuneable optical parametric oscillator (OPO) laser. In a new geometry [32], the laser beam intercepts the drifting ion in the drift tube. An ion gate halfway along the drift region allows the instrument to be used as a tandem ion mobility spectrometer, enabling mobility selection of ions prior to irradiation, with the photo-isomer ions being separated over the second half of the drift tube. The device uses a quadrupole for MS with a mass range of 100-440 Da.

We developed a new set-up to couple IMS capabilities with laser excitation. We took advantages of new instrument designs with ion funnels [14, 33-35] intercalated between two 79 cm long drift tubes. The first tube is used to resolve and select conformers, the selected ions are irradiated in the funnel between the two tubes and resulting species are dispersed in the second tube before mass analysis with a time-of-flight. Trapping of the ions in the funnel between the two tubes allows irradiation of ions for a selected amount of time as well as relaxation before separation in the second tube. Activation by collision is possible in the same region (between the two tubes) and between the second tube and the time-of-flight. The instrument is described in details below and its capability is demonstrated on IMS measurements of eosin anions and ubiquitin cations.

II. APPARATUS DESCRIPTION

A. GENERAL DESCRIPTION

Figure 1 gives an overview of the general design of the IMS-Laser-IMS apparatus. The overall length of the instrument is 3 m. The instrument has been developed based on a Maxis Impact (Bruker Daltonik, Bremen, Germany) quadrupole time-of-flight mass spectrometer (Q-Tof) that has been modified to serve as a detector after IMS measurements. Laser excitation is enabled by the injection of a light beam throughout the instrument, collinearly to the ions path.

From the left side on Figure 1, electrosprayed ions enter the source chamber and are guided to the first drift region (DT1) through a dual-stage ion Funnel assembly (A). The first stage of A (FunA1) is mainly used for transmission purpose, while the second stage (FunA2) can also

function as an ion trap. The second drift tube DT2 is identical to DT1, and separated from the latter by a dual-funnel assembly, denoted B, and similar to A (vida infra). The coupling to the Q-Tof is done through a third dual funnel assembly (C), followed by a stacked-ring radio-frequency (RF)-ion guide (IG), which conveys the ions to the original transfer optics of the Q-Tof.

The gas flows in the different regions of the instrument is carefully controlled in order to maintain a constant pressure in the drift region with no contamination from the air and solvent from the source capillary. Furthermore, an intermediate pressure region has been arranged between the drift region and the Q-Tof. This allows more flexible control of the drift pressure with minor impact on the residual pressure in the Q-Tof.

The three series of ion funnels and the two DT are housed in 9 aluminum chambers, electrically insulated from each other. To avoid possible electrical discharges, each chamber is floated at a DC voltage close to the one applied on the electrodes installed inside. The last chamber is grounded. The machining of mechanical parts was done by SMGOP company (38600 Fontaine, France).

B. **ELECTROSPRAY ION SOURCE**

The instrument has been designed to be used with Bruker Daltonik electrospray and captivespray sources. Results shown in this manuscript were obtained with the Apollo II electrospray source. The original source assembly was modified to be electrically insulated from the first chamber (which is floated at about 2 kV). The nebulizer needle is kept grounded, and the potential applied to the entrance of the transfer capillary is in the range 3-5 kV. This capillary is a 18 cm long glass capillary with a semiconductor coating on the inside diameter (Bruker Daltonik, inside diameter 0.5 mm, resistance 1000 MΩ). The potential at the exit of the capillary is typically 100-200 V higher than the one applied at the entrance of the first ion funnel (all voltages are given for the positive ion mode).

The source is mounted with a 50° angle relative to the instrument axis (see Figure 2). A stainless steel repeller electrode has been installed on the flange opposite to the source. It is maintained to a potential slightly higher than the one on the exit of the transfer capillary in order to maximize ion transmission to the first ion funnel.

The tilted geometry allows the injection of a laser through a 25.6 mm diameter window, mounted on the axis of the drift tubes. For UV and visible light injection, we used a 5 mm thick fused

silica window. Alternatively, a ZnSe window can be used for CO_2 infra-red laser beam. The design displayed on Figure 2 also allows mixing of two perpendicular laser beams by using a semi-reflective dichroic mirror instead of the on-axis window with an additional window on the side.

C. **DUAL-FUNNEL ASSEMBLIES**

The three dual-ion funnels denoted A, B, and C in Figure 1 were provided by Bruker Daltonics, together with their RF power supplies (QTIII Funnel Generator 1 and QTIII Funnel Generator 2). The electrical connections for RF and DC voltages were done using homemade vacuum feedthrough mounted on PEEK flanges.

The geometry of these dual ion funnels is sketched in the inset in Figure 1. They consist of stacks of 0.5 mm thick ring electrodes spaced by 0.5 mm and interconnected through 100 kΩ resistors. Opposite RF voltages are applied alternatively on adjacent electrodes. The first stage of the dual funnels is 6.5 cm long and the inner diameter of the electrodes varies from 45 mm to 1 mm. The second stage is 2.2 cm long and the inner diameter of the electrodes varies from 7.2 mm to 4 mm. The Base and Gate electrodes are DC-only. It can be used as an ion gate in FunA2, and FunB2, as described in section E. Its aperture is different for A, B, and C, related to the control of gas flows in the instrument (see section H). We added a 1 cm long DC-only ring electrode with 5 mm inner diameter at the end of the stacks for ion focusing (denoted Focus in Figure 1).

For each dual funnel assembly, the 7 different DC voltages (see Figure 1) are applied using high voltages power supplies (1, 2 and 3 kV HV modules, Iseg, Radeberg Germany). The values of the DC voltages, as well as the RFs amplitude and frequency are software controlled. The frequencies used are around 750 kHz, and 1230 kHz for stages 1, and 2 of the dual funnels, respectively, and typical DC voltages are given in Figure 3.

D. **DRIFT TUBES**

The two drift regions DT1, and DT2 are identical. Each drift tube is constructed with 3 sections that are assembled, yielding a total length of L=79 cm. The first section of DT1 is visible in Figure 2. Each section is composed of concentric stainless steel rings (15 cm o.d., 10 cm i.d.) that are isolated by 1 cm-thick PEEK spacers (1.5 cm o.d., 0.65 cm i.d.). The rings and spacers are stacked together on 3 PEEK rods. These rods are threaded at both ends, and the stack is maintained using PEEK nuts and Viton o-rings. O-rings are used to compensate for dilation

when varying the temperature of the tube. Each element is then mounted on rails fixed on the vacuum chambers. Electrical connections between adjacent sections, and to vacuum feedthroughs are provided by contacts between gold pins mounted on springs and brass plates attached to each DT section. A DC voltage is applied at the entrance and exit of each DT (see Figure 3). To ensure for a constant drift field, adjacent electrodes in the DT are connected through 75 kΩ resistors. Furthermore, 80% transmission Ni mesh is used at the first and last electrodes of each DT in order to maintain the field homogeneous on a well-defined distance.

E. PULSED VOLTAGES FOR IONS TRAPPING AND SELECTION

For IMS measurements, ions have to be injected at well-defined times in the drift tubes. Since the injection frequency is relatively low (typically 5 Hz), trapping ions between two IMS cycles considerably increases sensitivity. To this end, pulsed voltages can be applied on the last electrodes (further denoted GateA and GateB) of FunA2, and FunB2. Fast high voltage push-pull switches based on MOSFET circuits were developed in house (raise and fall times < 1µs). The opening time and duration of these ion gates are software-controlled through TTL signals.

Typical voltages used to trap cations in funnel FunB2 are given in the inset in Figure 3. The voltage drop across the funnel is typically 20 V. It depends on the ions to store. In trapping mode, the Gate voltage is set to a value close to the one applied to the first electrode of the funnel. In release mode, the gate voltage is decreased to a value slightly superior to the one on the last funnel electrode. The typical duration for ion release is 75 to 500 µs.

Tandem IMS measurements is performed by selecting ions with a given mobility at the end of DT1. This requires to select ions that reach the end of DT1 in a given time window. The selection is done by switching the entrance potential of FunB1. To discard the ions, it is set about 30 V higher (in the positive mode) than the one on the last electrode of DT1. During the selection window, it is lowered.

F. ION TRANSFER TO THE Q-TOF: ION FUNNEL AND ION GUIDE

The transfer from the end of DT2 to the entrance of the Q-Tof starts with FunC1 and FunC2 which are used for focalization of the ion beam exiting DT2. Coupling to the Q-Tof ion optics is achieved through a home-built stacked-ring RF ion guide (IG in Figure 1). It is composed of 40 identical stainless steel electrodes, i.d 5 mm, o.d 40 mm, 1 mm thick, and evenly spaced by 2 mm. Adjacent electrodes are connected through 500 kΩ resistors in order to apply a driving

DC field across the guide. Typical DC values are in the range 50-100 V. Opposite RF voltages are applied alternatively to adjacent electrodes through 10 pF HV capacitors. The 1.1 MHz RF is provided by a software controlled HF generator (QT ESIHEX, Bruker Daltonik). The amplitude of the RF field is kept relatively low (10 – 30 Vpp) in order to avoid collisional activation or ion trapping in the guide.

G. **Q-TOF**

The source of the Maxis Impact was moved at the entrance of the instrument (*vida supra*). The ions enter the Q-Tof through a dual ion funnel, which provides additional differential pumping stage and ion focusing before entering guiding optics. The funnels are followed by an hexapole, a quadrupole (mass range 20 – 40000 m/z, isolation up to 3000 m/z), a collision cell using N_2 as buffer gas and a high resolution Tof mass spectrometer (40000 resolution full sensitivity), that can be operated at up to 20 kHz. The pressure in the collision cell is kept low (~15 % of maximum value, about 10^{-2} mbar) to avoid trapping of ions in the cell. Voltages were adjusted to push forward the ions in the different parts of the Maxis Impact (in particular in the hexapole and quadrupole) to avoid any loss of IMS resolution due to ion trapping. Furthermore the ion optics setting are optimized in order to minimize activation energy at each step. Two detectors are available, one after the Tof and one on the axis of the instrument used to detect the ions without using the Tof (mass selection with the quadrupole).

H. **PUMPING AND GAS FLOWS**

The stability and control of pressures and gas flows is particularly critical in the instrument. Firstly, the pressure inside the drift region has to be stable and well defined, in order to determine collision cross section with accuracy. Second, contamination of He used as a drift gas by the air and solvent flowing from the source capillary has to be avoided as the mass of the drift gas is used for the collision cross section determination. Finally, the transfer of the ions from the relatively high pressure drift region, to the high vacuum required in the mass analyzer ($2x10^{-7}$ Torr) has to be done smoothly enough to minimize undesired collisional activation of the ions, while maintaining a good transmission. Smooth transfer conditions are particularly critical to allow studying loosely bound complexes, e.g. in the context of native MS [36-40].

The pressure in the drift tube is set constant by controlling the flow at the Helium inlet and the exhaust flow at both tube ends. Typical values given below correspond to a pressure of 12 Torr in the DTs. The inlet He flow (588 sccm) at the end of DT2 is regulated and monitored using a mass flow controller (SLA5850, Brooks, Hatfield, PA USA), which is software controlled. Pumping is achieved in the source region by 1 dry pump (ACP 28, Adixen), connected to the chamber via insulated tubing. A leak valve is used to control the outlet flow. In the transfer region to the Q-Tof, an intermediate pressure region has been designed to ensure for smooth pressure decrease towards high vacuum. It corresponds to the chamber that houses FunC2. This intermediate region and the first chamber of the Q-Tof are pumped by additional dry pumps (ACP 15, Adixen). The exhaust flows are adjusted via leak valves. In the intermediate chamber, a small nitrogen flow (92 sccm) is injected though a second mass flow controller. This enables to adjust the transfer pressure independently from the drift pressure.

The gas flow (mainly air) through the transfer capillary in the source region was estimated to be ~1000 sccm. To avoid contamination of the drift gas by the air from the source, the pressure in DTs chamber is maintained 0.4 Torr higher than the one in the source chamber. The limiting aperture between the two chambers is the last DC-electrode of FunA1, which has a 1 mm inside diameter. Under these conditions, the Helium counter flow through FunA1 was found to be sufficient to avoid drift gas contamination. This was confirmed by pressure-dependent IMS measurements (data not shown). The diameter of the limiting aperture at the other end of the drift region, namely the last DC electrode of FunC1, is 0.7 mm.

Pressures in the source, drift, and intermediate regions are monitored with digital capacitance manometers (CMX2T21 and CMX2T31, Brooks, Hatfield, PA USA) while pirani gauges (925 micropirani pressure transductor, MKS, Le Bourget, France) are used for lower pressure measurements and on each pump. Pumps are automatically shut down in case of a sudden pressure increase. Typical pressures in the different regions are as follows: 11.6 Torr in the source chamber, 12 Torr in the drift region, 0.750 Torr in the intermediate region (FunC2), 0.6 Torr in the Q-Tof transfer region. Finally, the pumping system of the Maxis Impact allows reaching 2.0×10^{-7} Torr in the Tof region.

I. TEMPERATURE

The chambers housing the two DTs were designed to allow a liquid flow within the thickness of the walls. To adjust the temperature, we use an external bath with an insulating silicon oil (SIL 180, ThermoFisher Scientific), which temperature can be varied from -20 to 100 °C using a

thermostated circulator (WCR-P30, Witeg Labortechnik GmbH, Wertheim, Germany). The temperature of the chambers is monitored with K-type thermocouples.

J. **LASER**

Experiments described in this manuscript were performed with a blue *cw* laser (488 nm, power 200 mW, Cobolt, Solna, Sweden). The laser is aligned on the axis of the instrument using two mirrors and injected through the window mounted on the source chamber. The beam diameter is 1 mm. The laser beam exits the instrument through an additional window on the chamber of the Tof via a 45° mirror mounted after the on axis detector (the detector was drilled at its center).

K. **ACQUISITION**

The original microchannel-plate detector of the Bruker instrument is used to detect the ions after the Tof. It is connected to a preamplifier and independently to two Agilent data acquisition boards: the original one from the Q-Tof, and an additional one (U1084A high-speed digitizer, Agilent Technologies, Santa Clara, USA). This latter board was added to handle IMS-MS acquisitions, which are more demanding than simple MS acquisitions (see below). The main characteristics of this board are: Memory 512 Mb, Dual channel, 2-4 GS/s, on-board signal averaging and processing.

Different acquisition modes are available. They rely on different sequences for the application of the pulsed voltages. Synchronization between the different pulses including the Tof pusher is software controlled.

Mass spectra can be recorded by using the Bruker software and turning off all triggers, but the one used for the Tof pusher. In this case, the Tof trigger is set to run continuously at the chosen frequency.

Figure 4 provides a typical timeline for an IMS-MS acquisition sequence. The ions are trapped in FunB2 and injected at t=0 in DT2. The Tof trigger is switched on after a delay τ_{TOF} and for a duration δ_{TOF}. This period is set to include the arrival time of the ions of interests. The mass range and sampling rate for the Tof spectra is defined through the parameters of the acquisition board. The board is triggered on the same signal as the Tof pusher. A series of n_{TOF} mass spectra (i_{TOF} = 1 to n_{TOF}) is recorded and stored on the Agilent board. The arrival time AT of the ions in the mass spectrum at index i_{TOF} is defined as:

$$AT = \boldsymbol{\tau_{TOF}} + \boldsymbol{i_{TOF}} * (\frac{\boldsymbol{\delta_{TOF}}}{\boldsymbol{n_{TOF}}}) \quad (1)$$

The same acquisition sequence is repeated after each injection of ions in DT2.

This yields 2-dimentional datasets. One dimension corresponds to AT and is related to the drift time in DT2. The number of bins is n_{TOF} and the bin width is δ_{TOF}/n_{TOF} (inverse of the Tof repetition rate). The other dimension is the time of flight of the ions in the Tof (which gives the *m/z* of the ions). The bin width in this dimension depends on the sampling rate chosen for the acquisition board. The size of the resulting dataset is limited by the size of the memory buffers, data processing times and transfer times. Note that time-of-flight were transposed to *m/z* values using ESI-L low concentration tuning mix (G1969-85000, Agilent Technologies, Santa Clara, CA, USA) for mass calibration.

For tandem IMS measurements, the acquisition sequence is given in Figure 5. The acquisition cycle begins with the injection of the ions from FunA2 to DT1. It is followed by the application of the selection, GateB and Tof pusher pulses. The final data has the same format as described above. Arrival times are referenced to GateB.

The results presented in Figures 8 and 9 were recorded by enabling laser irradiation in FunB2 after the selection pulse, and before injection in DT2, i.e. during trapping (see Figure 5).

L. ON AXIS DETECTION AND ACQUISITION

An alternate way to record arrival time distributions (ATDs) takes advantage of the on-axis dynode-coupled channeltron, located immediately after the Tof orthogonal extraction. The signal from this detector provides continuous monitoring of the integrated ATD for all ions. It can be used to record ATDs for ions with a given *m/z* value using the quadrupole for mass selection. The spectra are recorded using a preamplifier (9306, Ortec, Oak Ridge, TN, USA) and a multichannel scaler (Easy MCS, Ortec, Oak Ridge, TN, USA).

M. ELECTRONIC BOARDS AND CONTROL SOFTWARES

Three analog & digital input/output boards (NI PXI 6723, NI PXI 6225, NI PXI 6221, National instrument, Austin, TX USA) and timer counters PCI boards (NIPXI6602, National Instrument, Austin, TX USA) are used to drive the RF frequencies, mass flows and to generate the TTL synchronization pulses. Analog inputs allow monitoring of capacitance manometers, vacuum

gauges, and thermocouples. A home-made electronic board was specially designed for the interface between the PCI boards and the instrument for wiring purpose, to supply powers to the different parts and to provide various check points. The HV-power supplies are controlled via a local Ethernet network. The instrument voltages (including polarity), pressures, and temperatures (except voltages for the Q-Tof) are entirely controlled and monitored through home-made software developed using the wxWidgets graphical user interface library for C++[41]. The same software is used for controlling the Agilent board, the pulses and for data acquisition in the different modes described above. The original Q-Tof acquisition board and Q-Tof settings, except synchronization, are driven independently by the original Bruker control software (otofControl version 3.4).

III. **RESULTS**

A. **IMS MEASUREMENTS**

Figure 6a shows a mass spectrum obtained by electrospraying a solution of eosin Y ($C_{20}H_8Br_4O_5$, Sigma-Aldrich ref. E6003-25G) in the negative mode (100µM, in MeOH). The spectrum is dominated by doubly negatively charged eosin Y ($[M-2H]^{2-}$, *m/z* 321). Singly charge species is observed at *m/z* 643. The arrival time distribution (using the scheme in Figure 4) obtained for $[M-2H]^{2-}$ is shown in Figure 6b. A single peak is observed. The red line shows the time profile S(t) of the peak expected for a single isomer. It was calculated by convoluting the Gaussian lineshape from Fick's law for diffusion with a rectangular gate function of duration τ=75 µs that mimics the finite injection time at the tube entrance (GateB duration). This convoluted lineshape can be expressed as:

$$S(t) = \frac{I_0}{2}\left(\mathrm{erf}\left(\frac{t_d - t}{\delta} + \frac{\tau}{\delta}\right) - \mathrm{erf}\left(\frac{t_d - t}{\delta}\right)\right) \qquad (2)$$

where erf is the error function, I_0 is a normalization constant, and t_d is the average drift time of the ions. The diffusion parameter δ depends on t_d, and on the experimental drift voltage V and temperature T as [42] :

$$\delta = 2t_d\sqrt{\frac{k_B T}{qV}} \qquad (3)$$

where q stands for the charge of the ion, and k_B is the Boltzmann constant. The only free parameters used for fitting the experimental data are I_0 and t_d. In the case presented in Figure 6b, $\delta = 0.65\ ms$, which is significantly greater than τ. Consequently, the corresponding calculated

peak profile is nearly Gaussian, *i.e.* diffusion-limited. It reproduces the measured ATD. The experimental resolving power defined as t_d/FWHM is 40 for the singly charged species (figure 6b) (FWHM : full width at half-maximum). The calculated diffusion limited resolution at 500V is 41.9 for the singly charged ions and 59.2 for the doubly charged ions. Note that for short drift times, diffusion in the different RF-based ion optics between the end of DT2 and the detector may also reduce the resolution.

AT measured as a function of the inverse voltage value across DT2 for $[M-2H]^{2-}$ and $[M-H]^{-}$ are plotted in figure 6c. The reported values were determined by fitting the experimental ATDs using the profile from equation 4. The collision cross sections Ω can be extracted from the slopes of these curves [42]:

$$AT = t_0 + \frac{16}{3}\sqrt{\frac{\mu k_B T}{2\pi}}\frac{NL^2}{q\Omega}\frac{1}{V} \qquad (4)$$

with μ the reduced mass for ion-buffer gas collisions, N the number density of the buffer gas, and L the drift length. t_0 corresponds to the transfer time of the ions from the end of the DT2 to the detector. It depends on the mass, charge, and to some extent, mobility of the ions, but is independent of the drift field. The second term in the right-hand side of equation 4 is inversely proportional to Ω. From a linear fit on the experimental values on Figure 6c, the values of Ω and error bars deduced from the slope of the fit were 148.3 ± 0.1 $Å^2$ and 139.5 ± 0.4 $Å^2$ for doubly and singly charged species, respectively. The corresponding t_0 were found to be 3.51±0.01 ms and 6.52±0.07 ms for $[M-2H]^{2-}$ and $[M-H]^{-}$, respectively. Note that the change in charge state results in a significant change in collision cross section.

B. IMS-IMS EXPERIMENTS: UBIQUITIN

Ubiquitin was purchased from Sigma Aldrich (ref. U6253-25MG), and directly sprayed in a water/methanol 1/1 solution, with 1% acetic acid, at a concentration of 12 µmol.L^{-1}. In the following, we focus on the $[Ubiquitin+7H]^{7+}$ ions, further denoted U7. The ATD in Figure 7a was extracted from an IMS-MS map recorded with a drift pressure of 5.5 Torr, and a drift voltage of 580 V across DT2. Three main conformational families are resolved for U7 under those experimental conditions. [43, 44] Those families are labelled U7A, U7B, and U7C in Figure 7, in increasing order of drift time. Using the procedure described in the previous section, average cross section values could be determined for those 3 families. We found Ω of 1192±33 $Å^2$, 1441±51 $Å^2$, and 1552±23 $Å^2$ for U7A, U7B, and U7C, respectively.

The ATDs in Figure 7b were recorded in the IMS-IMS mode, as described in section K, Figure 5. Different selection windows, in order to select one of the three conformational families, were used. For those measurements the delay between the selection pulse and the injection in DT2 was kept constant at 10 ms. These ATDs display a single feature: U7A for the black line, U7B for the green line, and U7C for the blue line. Selection of a conformational family was successively achieved. The observed peaks are wider than the selection window. This broadening is attributed both to diffusion in DT2 and to inter-conversion between the different conformers that compose the identified conformational families. In contrast, only diffusion broadening was observed after selection in the case of the very rigid eosin Y ions (see next section).

As shown by Clemmer and co-workers on triply-charged bradykinin [17], collisional excitation can be used in tandem IMS experiments to trigger transitions between different structural families. This can be achieved after the first IMS stage in our setup by increasing the voltage drop between FunB1 and FunB2. Figure 7c displays ATDs recorded after selection of U7A at the end of DT1. If the voltage drop is 4 V, the recorded ATD shows a single peak corresponding to U7A. As the voltage drop is increased to 94 V, a significant part of the ions is detected with drift times corresponding to U7B. Finally, with a voltage of 134 V, the ATD is very similar to the one obtained when selecting U7C. This is expected if ubiquitin unfolds under activation and similar to what was observed by Clemmer and co-workers though their resolution is better due to the use of higher drift voltages [45] In addition, our experiments were performed at low pressure to facilitate collisional activation. As already mentioned, at low pressure in the DT (short drift times), diffusion in ion optics after DT2 may have an effect on the observed resolution.

C. IMS-LASER-IMS EXPERIMENTS: PHOTO-OXIDIZED EOSIN

IMS-Laser-IMS experiments were performed on eosin Y. The (AT / *m/z*) map obtained after selection of $[M-2H]^{2-}$ species is shown in Figure 8b. Doubly charged ions were selected with a width of 500 µs in FunB1, trapped for 6 ms in FunB2 and then injected in DT2 for the second ion mobility stage. The map is dominated by a single peak corresponding to the doubly charged eosin Y. Figure 8a was obtained with the same experimental conditions, excepted that the ions were irradiated at λ=488 nm for 1 ms while they were trapped in FunB2. The synchronization of ion trapping and laser beam allows analyzing only selected ions, and their photo-fragments, in DT2. The map shows a new peak at *m/z* 646 and AT corresponding to the one observed for the singly charged species. As shown in the inset of Figure 8a, the isotopic pattern corresponds to the

one expected for the $[M-2H]^-$ radical ion. Irradiation of $[M-2H]^{2-}$ induced an electron photo detachment [46, 47] and formation of $[M-2H]^{-\cdot}$ ions. Measurement of the AT as a function of the voltage across DT2 leads to a collision cross-section of 137.9±0.4 $Å^2$ for these radical ions. This value is within the error bar of the value measured for the non-radical species showing that the loss of one hydrogen atom does not result in a significant change in the collision cross section contrary to what was observed between singly and doubly deprotonated species.

Figure 9 shows the intensity of $[M-2H]^{2-}$ species recorded as a function of irradiation time (IMS-Laser-IMS measurements). The trapping time in FunB2 (δt_{Trap} on Figure 5) was fixed to 3 ms and the irradiation time varied from 0 ms to 3 ms. As expected from equation 5 it shows a linear increase:

$$\ln\left(\frac{I_0}{I}\right) \propto \sigma\varphi t \qquad (5)$$

where σ is the absorption cross section of the molecular ion, t is the laser irradiation time and φ is the laser power. At 3ms, 86 % of the ions has been depleted.

IV. **SUMMARY AND OUTLOOK**

We described a new experimental set-up to perform tandem ion mobility spectrometry measurements coupled to time of flight high resolution mass spectrometry. This instrument allows recording IMS-MS maps. Alternatively one can record IMS data for a selected ion using an on-axis detector, the ion being mass selected with the quadrupole. The geometry of the instrument allows to select ions according to their ion mobility, activate them and examine the ion mobility of the product ions. IMS-IMS experiments on Ubiquitin are reported. We selected a given isomer of charge state +7 and explored its structural rearrangement following collisional activation between the two drift tubes. The set up was built to permit a laser irradiation of the ions in the transfer region between the two drift tubes. In particular, the source is off-axis to perform on-axis laser irradiation. The synchronization of the laser beam and ion pulses allows to irradiate selected ions for a controlled amount of time. An example of IMS-Laser-IMS experiment was reported on eosin Y, where laser irradiation was used to produce radical ions by electron photodetachment starting from doubly deprotonated ions. We checked that the electron-detachment yield is proportional to the irradiation time. This set-up allows to perform photo-excitation on selected isomers and also to measure collision cross section of photo-products, which cannot be directly produced with an electrospray source. Ongoing experiments include coupling of ion mobility experiments with action-FRET measurements [48, 49].

ACKNOWLEDGMENTS

The research leading to these results has received funding from the European Research Council under the European Union's Seventh Framework Programme (FP7/2007-2013 Grant agreement N°320659). We acknowledge Oliver Räther, Jean-Michel Billmann and Claude Marfisi from Bruker Daltonik for technical support and Serge Vialet (SMGOP) for fruitful discussions during the design of the instrument.

REFERENCES

[1]D. F. Hagen, Anal. Chem. **51,** 870 (1979).
[2]G. von Helden, M. T. Hsu, N. Gotts and M. T. Bowers, J. Phys. Chem. **97,** 8182 (1993).
[3]D. E. Clemmer and M. F. Jarrold, J. Mass Spectrom. **32,** 577 (1997).
[4]M. F. Mesleh, J. M. Hunter, A. A. Shvartsburg, G. C. Schatz and M. F. Jarrold, J. Phys. Chem. **100,** 16082 (1996).
[5]T. Wyttenbach, G. von Helden, J. J. Batka Jr, D. Carlat and M. T. Bowers, J. Am. Chem. Soc. Mass Spectrom. **8,** 275 (1997).
[6]A. Politis, A. Y. Park, S.-J. Hyung, D. Barsky, B. T. Ruotolo and C. V. Robinson, PLoS ONE **5,** e12080 (2010).
[7]T. Wyttenbach, G. von Helden and M. T. Bowers, J. Am. Chem. Soc. **118,** 8355 (1996).
[8]R. R. Hudgins, P. Dugourd, J. M. Tenenbaum and M. F. Jarrold, Phys. Rev. Lett. **78,** 4213 (1997).
[9]M. F. Jarrold, Acc. Chem. Res. **32,** 360 (1999).
[10]J. Woenckhaus, Y. Mao and M. F. Jarrold, J. Phys. Chem. B **101,** 847 (1997).
[11]J. A. Silveira, K. A. Servage, C. M. Gamage and D. H. Russell, J. Phys. Chem. A **117,** 953 (2013).
[12]B. Gao, T. Wyttenbach and M. T. Bowers, J. Am. Chem. Soc. **131,** 4695 (2009).
[13]J. Woenckhaus, R. R. Hudgins and M. F. Jarrold, J. Am. Chem. Soc. **119,** 9586 (1997).
[14]S. L. Koeniger, S. I. Merenbloom, S. J. Valentine, M. F. Jarrold, H. R. Udseth, R. D. Smith and D. E. Clemmer, Anal. Chem. **78,** 4161 (2006).
[15]S. I. Merenbloom, S. L. Koeniger, S. J. Valentine, M. D. Plasencia and D. E. Clemmer, Anal. Chem. **78,** 2802 (2006).
[16]H. L. Li, B. Bendiak, W. F. Siems, D. R. Gang and H. H. Hill, Anal. Chem. **85,** 2760 (2013).
[17]N. A. Pierson, S. J. Valentine and D. E. Clemmer, J. Phys. Chem. B **114,** 7777 (2010).
[18]S. Lee, S. J. Valentine, J. P. Reilly and D. E. Clemmer, Int. J. Mass Spectrom. **309,** 161 (2012).
[19]T.-Y. Kim, S. J. Valentine, D. E. Clemmer and J. P. Reilly, J. Am. Chem. Soc. Mass Spectrom. **21,** 1455 (2010).

[20]S. Zucker, S. Lee, N. Webber, S. Valentine, J. Reilly and D. Clemmer, J. Am. Chem. Soc. Mass Spectrom. **22,** 1477 (2011).
[21]K. Koyasu, T. Ohtaki, N. Hori and F. Misaizu, Chem. Phys. Lett. **523,** 54 (2012).
[22]B. Bellina, J. M. Brown, J. Ujma, P. Murray, K. Giles, M. Morris, I. Compagnon and P. E. Barran, Analyst **139,** 6348 (2014).
[23]R. Fromherz, G. Ganteför and A. A. Shvartsburg, Phys. Rev. Lett. **89,** 083001 (2002).
[24]M. Vonderach, O. T. Ehrler, P. Weis and M. M. Kappes, Anal. Chem. **83,** 1108 (2011).
[25]M. Vonderach, M.-O. Winghart, L. MacAleese, F. Chirot, R. Antoine, P. Dugourd, P. Weis, O. Hampe and M. M. Kappes, Phys. Chem. Chem. Phys. **16,** 3007 (2014).
[26]M. Vonderach, O. T. Ehrler, K. Matheis, T. Karpuschkin, E. Papalazarou, C. Brunet, R. Antoine, P. Weis, O. Hampe, M. M. Kappes and P. Dugourd, Phys. Chem. Chem. Phys. **13,** 15554 (2011).
[27]S. Warnke, C. Baldauf, M. T. Bowers, K. Pagel and G. von Helden, J. Am. Chem. Soc. **136,** 10308 (2014).
[28]G. Papadopoulos, A. Svendsen, O. V. Boyarkin and T. R. Rizzo, J. Am. Chem. Soc. Mass Spectrom. **23,** 1173 (2012).
[29]G. Papadopoulos, A. Svendsen, O. V. Boyarkin and T. R. Rizzo, Faraday Discuss. **150,** 243 (2011).
[30]N. J. A. Coughlan, B. D. Adamson, K. J. Catani, U. Wille and E. J. Bieske, J. Phys. Chem. Lett. **5,** 3195 (2014).
[31]B. D. Adamson, N. J. A. Coughlan, R. E. Continetti and E. J. Bieske, Phys. Chem. Chem. Phys. **15,** 9540 (2013).
[32]B. D. Adamson, N. J. A. Coughlan, P. B. Markworth, R. E. Continetti and E. J. Bieske, Rev. Sci. Instrum. **85,** 123109 (2014).
[33]S. A. Shaffer, D. C. Prior, G. A. Anderson, H. R. Udseth and R. D. Smith, Anal. Chem. **70,** 4111 (1998).
[34]B. H. Clowers, Y. M. Ibrahim, D. C. Prior, W. F. Danielson, M. E. Belov and R. D. Smith, Anal. Chem. **80,** 612 (2008).
[35]P. R. Kemper, N. F. Dupuis and M. T. Bowers, Int. J. Mass Spectrom. **287,** 46 (2009).
[36]C. Uetrecht, I. M. Barbu, G. K. Shoemaker, E. van Duijn and A. J. R. Heck, Nat. Chem. **3,** 126 (2011).
[37]Y. Gordiyenko, C. Schmidt, M. D. Jennings, D. Matak-Vinkovic, G. D. Pavitt and C. V. Robinson, Nat. Commun. **5,** (2014).
[38]S. L. Bernstein, N. F. Dupuis, N. D. Lazo, T. Wyttenbach, M. M. Condron, G. Bitan, D. B. Teplow, J.-E. Shea, B. T. Ruotolo, C. V. Robinson and M. T. Bowers, Nat. Chem. **1,** 326 (2009).
[39]R. R. Hudgins and M. F. Jarrold, J. Am. Chem. Soc. **121,** 3494 (1999).
[40]F. Canon, R. Ballivian, F. Chirot, R. Antoine, P. Sarni-Manchado, J. Lemoine and P. Dugourd, J. Am. Chem. Soc. **133,** 7847 (2011).
[41]*wxWidgets version 2.8.12, http://www.wxwidgets.org,* (released 2011).
[42]H. E. Revercomb and E. A. Mason, Anal. Chem. **47,** 970 (1975).
[43]T. Wyttenbach and M. T. Bowers, J. Phys. Chem. B **115,** 12266 (2011).
[44]S. Myung, E. R. Badman, Y. J. Lee and D. E. Clemmer, J. Phys. Chem. A **106,** 9976 (2002).
[45]H. L. Shi, N. Atlasevich, S. I. Merenbloom and D. E. Clemmer, J. Am. Chem. Soc. Mass Spectrom. **25,** 2000 (2014).
[46]R. Antoine, J. Lemoine and P. Dugourd, Mass Spectrom. Rev. **33,** 501 (2014).
[47]R. Antoine, L. Joly, T. Tabarin, M. Broyer, P. Dugourd and J. Lemoine, Rapid Commun. Mass Spectrom. **21,** 265 (2007).
[48]S. Daly, F. Poussigue, A.-L. Simon, L. MacAleese, F. Bertorelle, F. Chirot, R. Antoine and P. Dugourd, Anal. Chem. **86,** 8798 (2014).
[49]S. Daly, A. Kulesza, F. Poussigue, A.-L. Simon, C. M. Choi, G. Knight, F. Chirot, L. MacAleese, R. Antoine and P. Dugourd, Chem. Sci.**,** (2015).

FIGURE CAPTIONS

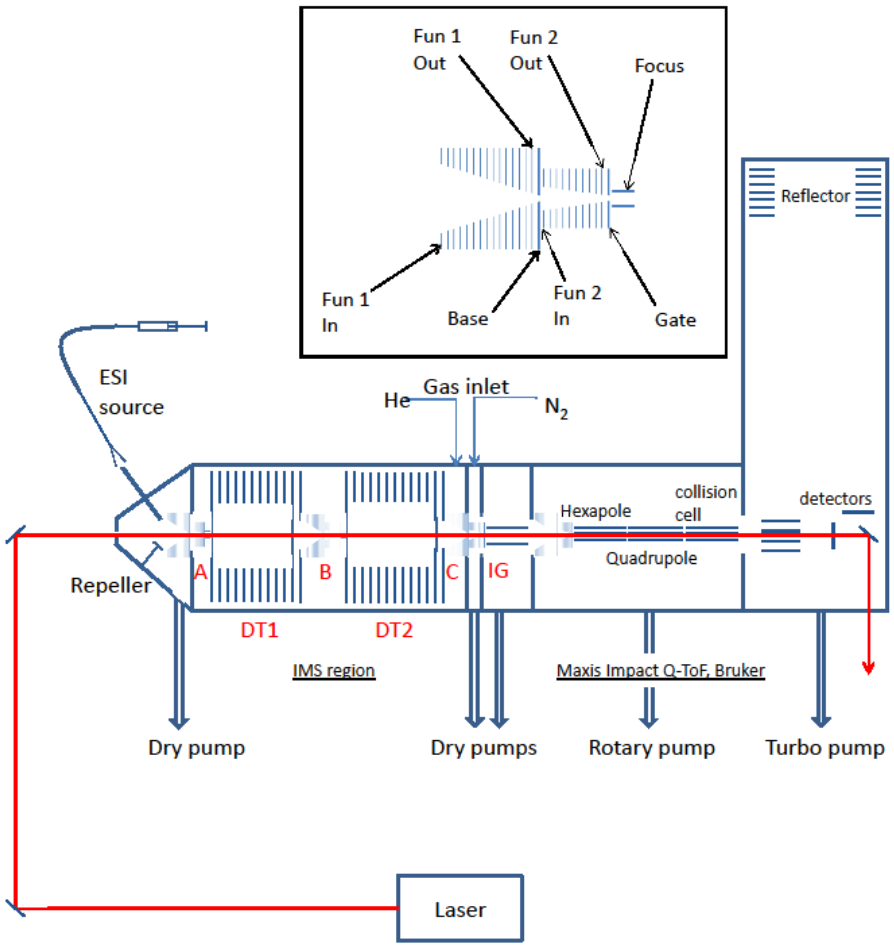

Figure 1. General scheme of the apparatus. The inset details the dual-ion funnel assembly, denoted A, B, and C on the general scheme. The fourth funnel is the one implemented in the commercial Maxis Impact (Bruker).

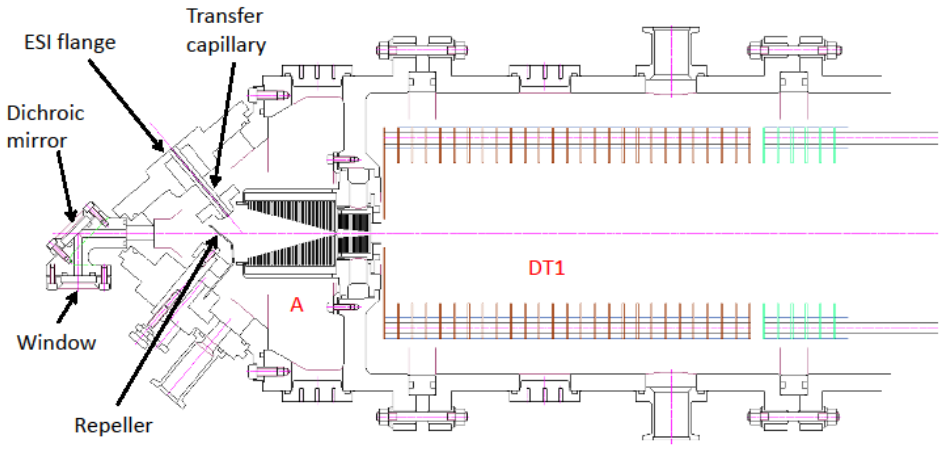

Figure 2. Mechanical drawing of the source chamber with off-axis transfer capillary to allow laser injection parallel to the drift tubes. A labels FunA1 and FunA2. DT1 labels the first section of DT1.

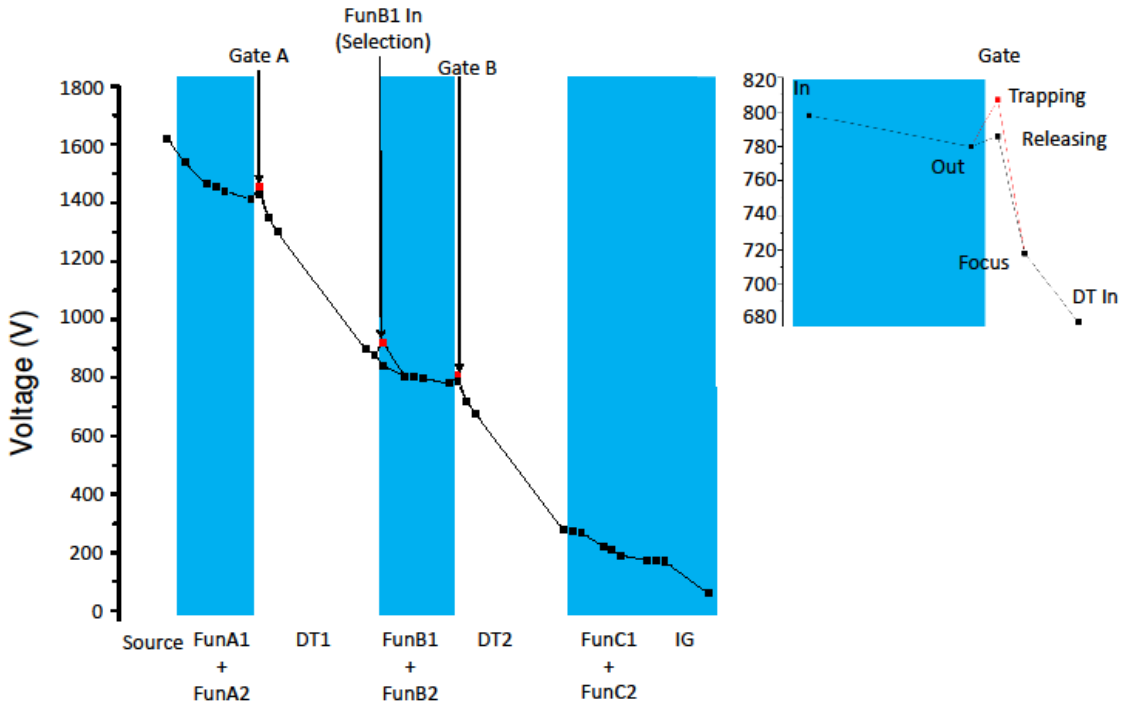

Figure 3. Examples of voltages used in the instrument for positive ions, from the source chamber to the ion guide. The red squares correspond to the high values for the three pulsed voltages. The shaded regions correspond to the ion funnel assemblies and to the transfer ion guide, where radiofrequencies are applied. The inset is a zoom on FunB2.

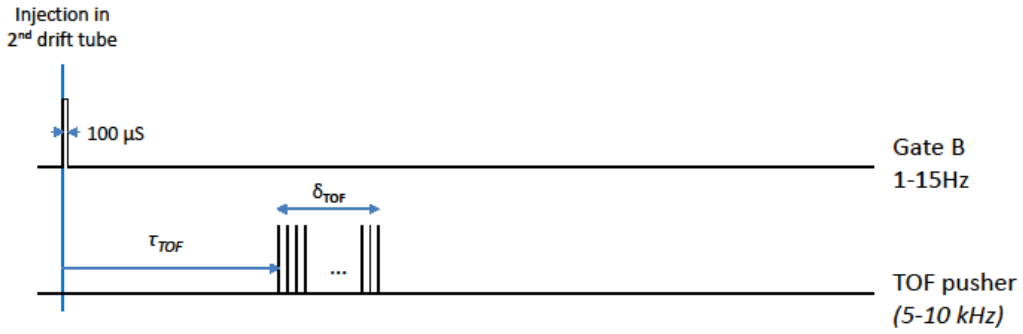

Figure 4. Timeline for IMS-MS cycles.

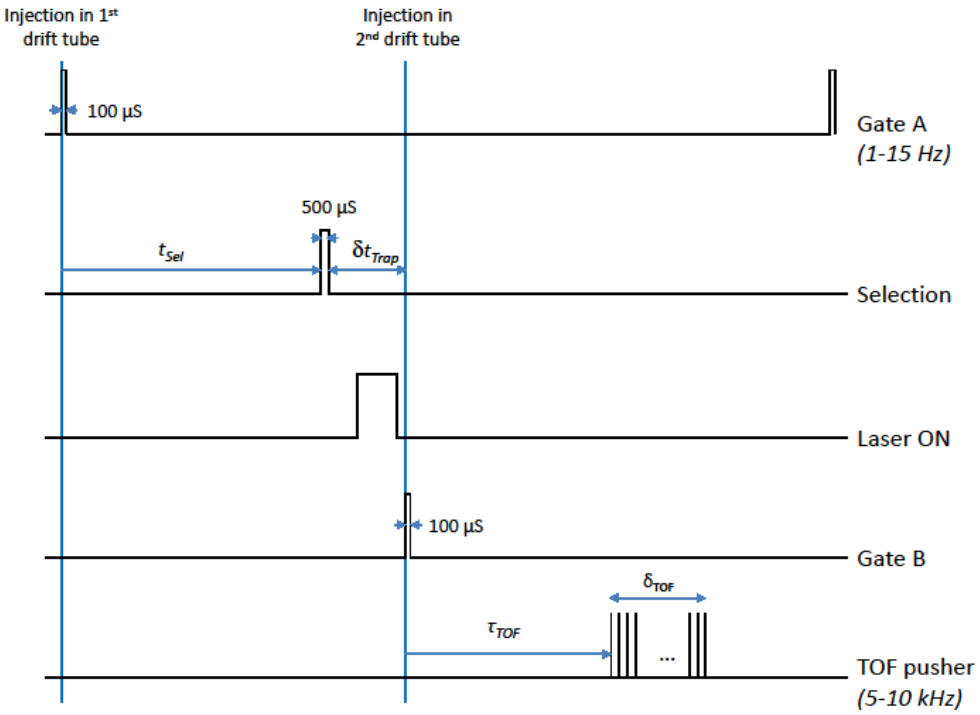

Figure 5. Timeline for IMS-Laser-IMS-MS cycles

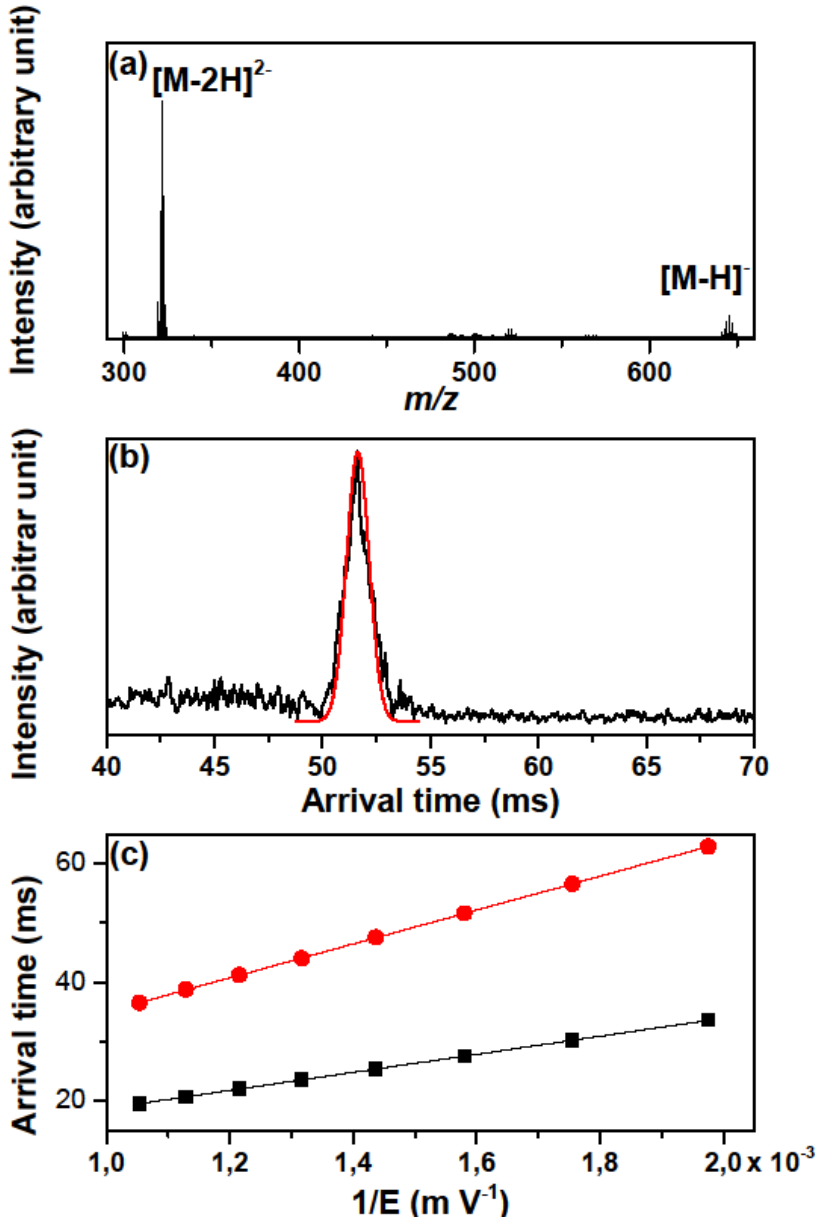

Figure 6. (a) Mass spectrum recorded in negative mode for Eosin Y. (b) ATD recorded for singly-deprotonated Eosin Y at a pressure of 11.62 Torr, a temperature of 300 K and a drift voltage of 500V across DT2 (black line). The calculated profile for a single conformer is plotted as a red line. The corresponding experimental resolving power is 40. (c) Arrival time as a function of the inverse drift voltage for singly- (red circles), and doubly-charged Eosin Y (black squares). The cross-section are extracted from a linear fit of these curves (solid lines).

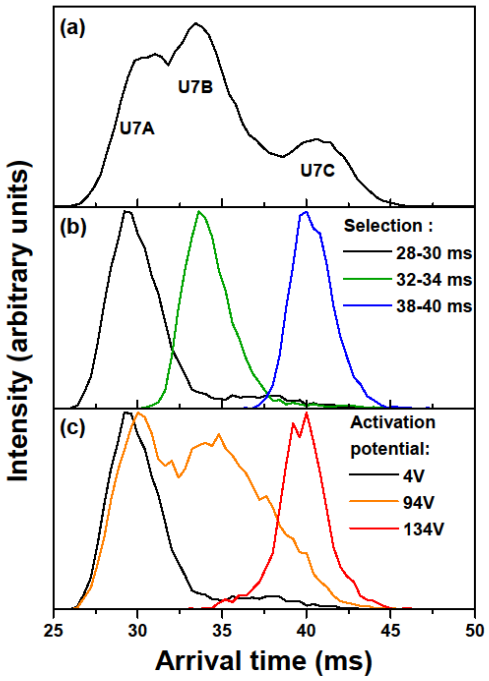

Figure 7. ATDs recorded for Ubiquitin7+ (drift pressure: 5.5 Torr, temperature: 300 K, drift voltages in DT1 and DT2: 580 V). (a) DT2 only (no selection, see Figure 4). (b) DT1 and DT2, with three different selection windows after DT1 (see Figure 5). (c) DT1 and DT2, with selection of isomer A and collisional activation in FunB1. Activation is obtained by increasing the voltage drop between FunB1 and FunB2.

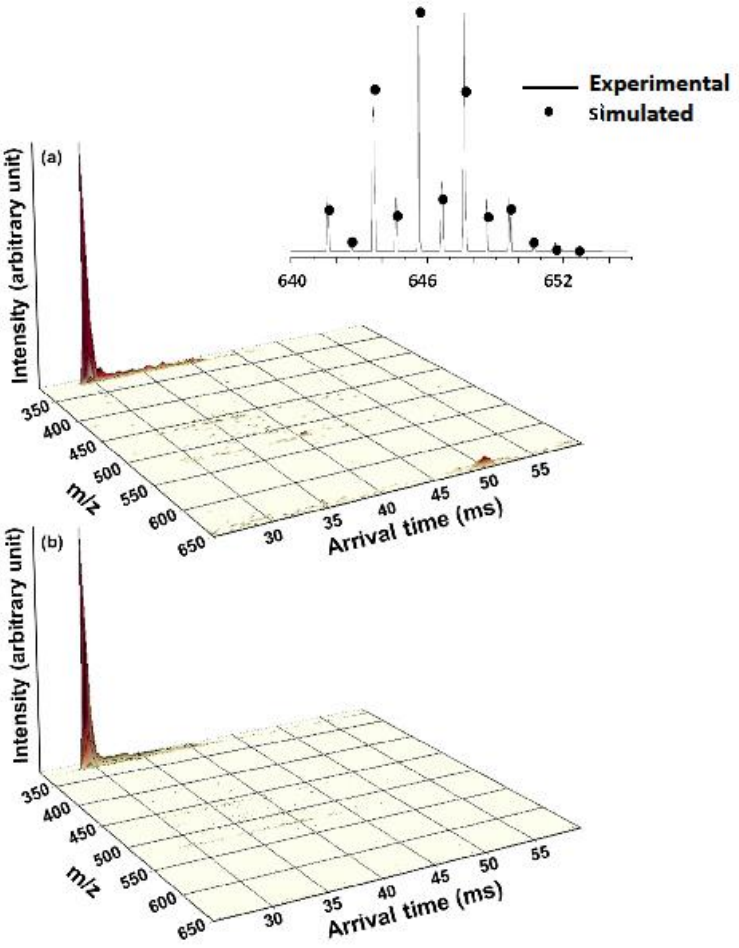

Figure 8. IMS-MS maps recorded after selection of doubly charged Eosin Y after DT1 without (bottom), and with (top) laser irradiation in FunB2 (10 ms irradiation time, λ=488 nm) (p= 11.6 Torr, T= 300K, V= 570 V). The inset is a zoom on the isotopic pattern of the singly charged photoproduct (solid line: Exp., dots: calculated pattern for radical $[M-2H]^{\cdot}$ ions).

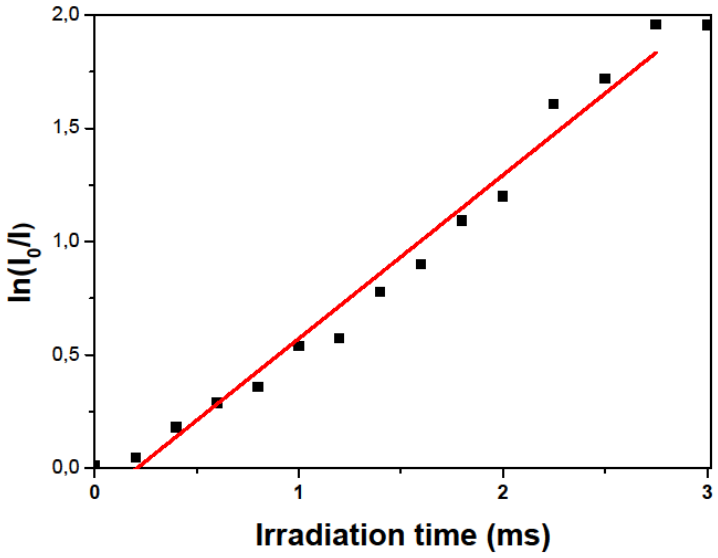

Figure 9. Ratio of doubly-charged Eosin Y intensity without (I_0) and with (I) laser irradiation in FunB2 as a function of the irradiation time. The red line is a guide for the eyes.